Medium-Term Prediction of Chaos

Chris Strelioff and Alfred Hübler
Center for Complex Systems Research, Department of Physics,
University of Illinois at Urbana-Champaign,
1110 West Green Street, Urbana, Illinois 61801
(Dated: July 19, 2005)

We study prediction of chaotic time series when a perfect model is available but the initial condition is measured with uncertainty. A common approach for predicting future data given these circumstances is to apply the model despite the uncertainty. In systems with fold dynamics, we find prediction is improved over this strategy by recognizing this behavior. A systematic study of the Logistic map demonstrates prediction of the most likely trajectory can be extended three time steps. Finally, we discuss application of these ideas to the Rössler attractor.

PACS numbers: 05.45.Ac,05.45.Pq,05.45.Tp

Development of methods for prediction and characterization of time series continues to be an active area of research [1–3]. In particular, methods developed for analyzing chaotic dynamics have an increasing number of applications. Some representative examples include prediction of epileptic seizures [4], analysis of population dynamics in ecology [5], prediction of equipment failure [6], and understanding error in weather prediction [7, 8]. Much of the fundamental research on chaotic time series focuses on two general ideas. The first is inference of model parameters for prediction of future data [9–11]. In general this is effective for short-term description of the system. The second approach focuses on estimation of average quantities or an invariant measure for classification of long-term behavior [12, 13].

We propose an extension of these viewpoints by incorporating ideas from both short and long-term approaches. We treat the initial condition as a measurement with uncertainty, resulting in an initial probability density function (pdf). While propagation of a probability density with underlying chaotic dynamics has been studied analytically [14, 15], a direct connection to prediction of time series has not been made to our knowledge. Our goal is to use an understanding of pdf dynamics to indentify the most probable trajectory.

We find prediction of a trajectory using these ideas to be very effective in systems with fold dynamics. Two well known examples of chaotic systems with this behavior are the Logistic map [16] and Rössler attractor [17]. A perfect model, using an initial condition measured with uncertainty, will not accurately describe the most probable trajectory beyond the short-term in these systems. The evolution of the initial pdf will develop new peak(s) due to the fold dynamics. These peaks are generally not related to images of the measured value and prediction of a trajectory begins to fail. Recognition of this effect is the key to extending prediction of a trajectory into the medium-term regime.

This Letter is organized as follows. First, we describe a general one dimensional map and the properties necessary to produce fold dynamics. Next, we introduce a model of measurement with uncertainty which produces an initial pdf . We then consider evolution of an ensemble of trajectories consistent with this measurement. This material motivates the proposed prediction method and a systematic numerical study of our approach verifies its effectiveness. Finally, the extension of these ideas are discussed for higher dimensional systems. In particular, we discuss the application of the proposed method to the Rössler attractor.

To illustrate the basic ideas of our method, we focus on a 1-dimensional map

$$x_{n+1} = f(x_n, a). \tag{1}$$

We require $f(x, a)$ be differentiable on its domain with one or more critical points, x_c^i, which must satisfy $f'(x_c^i, a) = 0$ and $f''(x_c^i, a) \neq 0$. As an example we introduce the Logistic map, defined $f(x, a) = ax(1 - x)$, where $a \in [0, 4]$ and $x \in [0, 1]$. For this map, we have $f'(x_c, a) = 0$ at $x_c = 1/2$, and $f''(x_c, a) = -2a$.

The first step in prediction, given a model of the dynamics, is specification of an initial condition. We propose the following model for measurement. The relationship between the true initial state, x, and the measured value, m, is given by $m = x + r$. The uncertainty in the measurement is reflected by r, with probability density $\rho(r)$. We will use a unimodal function, such as the normal distribution with mean zero and small variance. This choice is designed to model random, non-systematic uncertainty. The resulting form is a distribution consistent with the measured value and type of uncertainty assumed. To ease future notation, we will write this initial pdf as $\rho_0(x)$.

The range of possible trajectories which can be followed by an initial condition with measurement uncertainty are investigated by constructing an ensemble. The first step is to generate a set of n_d initial conditions, $\{x_j | j = 0, 1, \ldots, n_d - 1\}$, consistent with the type of measurement uncertainty assumed above. The time evolution of each x_j with Eq. (1) is used to produce the set of possible trajectories, $\{f^{(n)}(x_j, a)\}$. We use the notation $f^{(n)}(x, a)$ to indicate n applications of the map to x.

A histogram is constructed from the ensemble to provide a coarse-grained approximation of the pdf, $\rho_n(x)$. The region of interest is divided into n_b equally sized bins labeled $\mathcal{B}_i = [x_{min} + iW_i, x_{min} + (i+1)W_i)$, where $i = 0, 1, \ldots, n_b - 1$. The width of each bin is $W_i = (x_{max} - x_{min})/n_b$, where x_{min} and x_{max} are the minimum and maximum of $\{f^{(n)}(x_j, a)\}$ for all x_j and n. In this way, the bins cover the region of interest, $\cup_i \mathcal{B}_i = [x_{min}, x_{max}]$. The complete histogram at time n is given by

$$H_n(x) = \sum_{i=0}^{n_b-1} H_{n,i}\, \mathbb{1}_{\mathcal{B}_i}[x], \tag{2}$$

where the estimated probability density for $\mathcal{B}_i$ at time n is

$$H_{n,i} = \frac{n_b}{n_d} \sum_{j=0}^{n_d-1} \mathbb{1}_{\mathcal{B}_i}[f^{(n)}(x_j, a)]. \tag{3}$$

In the above equations, $\mathbb{1}_{\mathcal{B}_i}[x] = 1$ if $x \in \mathcal{B}_i$ and is zero otherwise. The value given in Eq. (3) is associated with the center of the bin, given by $x_i = x_{min} + (i + 1/2)W_i$. The path followed by the largest fraction of the ensemble identifies the most-likely trajectory at each time step and is associated with the bin with largest probability density, $H_{n,i}$.

Fig. (1) provides an illustration of typical dynamics for the Logistic map at $a = 3.80$, a value which produces chaotic dynamics. For this example, the ensemble of initial conditions is distributed as $x_j \sim \mathrm{N}(m_0, \sigma_0)$, where $m_0 = 0.91$ and $\sigma_0 = 5 \times 10^{-3}$. The values $n_d = 10^6$ and $n_b = 10^3$ were used in construction of the ensemble and histogram. In the short-term regime, $n \leq 3$ in this example, the histogram remains approximately normal and the most likely value for x is accurately described by images of the measured value, $f^{(n)}(m_0, a)$. We also note the standard deviation increases with time, $\sigma_{n+1} \approx |f'[f^{(n)}(m_0, a), a]|\sigma_n$, reflecting a growth in the uncertainty of the most likely value.

At $n = 3$ there is a significant probability the measured value will be near the critical point (a quantitative test will be introduced below). A new peak in the histogram is created at the image of the critical point, $f(x_c, a)$, at the next time step. For time $4 \leq n \leq 7$, following this new peak accurately describes the most likely trajectory. By time $n = 7$, the path followed by m_0 has an error equal to approximately twenty percent of the attractor size.

The origin of the new peak can be understood by introducing the Frobenius-Perron operator, which describes

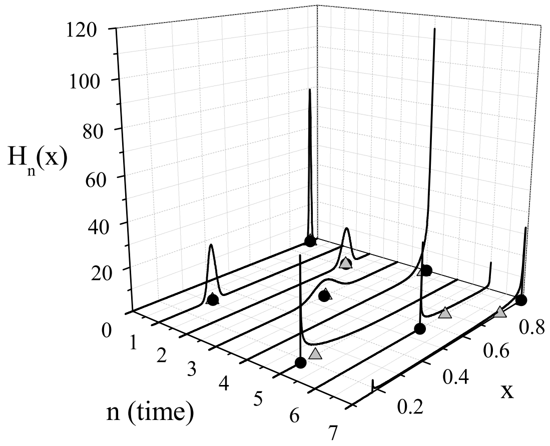

FIG. 1: An example of evolution of an initial condition with uncertainty. The underlying map dynamics are governed by the Logistic map at $a = 3.80$, resulting in chaotic dynamics. At each time step a histogram is shown along with the trajectory of the initial measurement, $f^{(n)}(m_0, a)$ (gray triangle), and the most likely trajectory (black circle). At time $n = 7$ the error in prediction produced by following $f^{(n)}(m_0, a)$ is approximately twenty percent of the attractor size.

the time evolution of a probability density driven by map dynamics. For the noise-free map dynamics, as described in Eq. (1), a general form for the operator can be written

$$\rho_{n+1}(x) = \sum_j \frac{\rho_n[f_j^{(-1)}(x, a)]}{|f'[f_j^{(-1)}(x, a), a]|}. \tag{4}$$

The sum is over all inverses j of the map given by $x_n = f_j^{(-1)}(x_{n+1}, a)$. The requirements for Eq. (1) have clear implications for the resulting evolution of the probability density. The denominator in Eq. (4) can be equal to zero. As a result, if the probability density overlaps a critical point at time n a singularity will be created at time $n+1$. This is the origin of the new peak in Fig. (1). As discussed in [18], the ill-behaved singularity in an exact mathematical treatment appears as a smoothed peak in a histogram which reflects measurement with finite resolution.

The key to extending prediction is to recognize cases when the probability density near the critical point(s) is sufficient to create a new peak. For this purpose, we define a ratio

$$\mathcal{R}_n^i = \frac{\int_{x \in n[f(x_c^i, a)]} dx\ \rho_{n+1}(x)}{\int_{x \in n[f(\mu_n, a)]} dx\ \rho_{n+1}(x)}. \tag{5}$$

This ratio compares the probability associated with a small region near the image of the critical point, which we label $n[f(x_c^i,a)]$, to the probability in a small region near the image of the current most probable state, $n[f(\mu_n,a)]$.

Motivated by the observations in Fig. (1) and knowledge of the probability density dynamics given in Eq. (4), we propose the approximation $\rho_n(x) \approx \mathrm{N}(x;\mu_n,\sigma_n)$. This is not meant to be an accurate representation of the true probability density. Rather, this approximation serves as a tool for recognition of folds which will create new peaks. In this spirit, the dynamics of the most likely point, μ_n, and standard deviation of the density, σ_n, are given by

$$\mu_{n+1} = \begin{cases} f(\mu_n,a) & \mathcal{R}_n^i < 1 \\ f(x_c^i,a) & \mathcal{R}_n^i \geq 1, \end{cases} \tag{6a}$$

$$\sigma_{n+1} = |f'(\mu_n,a)|\sigma_n. \tag{6b}$$

We set the initial values to reflect the measurement with uncertainty, $\mu_0 = m_0$ and σ_0^2 reflecting the variance in $\rho(r_0)$. We expect that this approximation is only effective in the short and medium-term regimes, reflected by a small value for σ_n. In practice, the presence of multiple pronounced peaks in the histogram reflects the end of meaningful trajectory prediction.

For application of Eq. (6), a reasonable approximation for $\mathcal{R}_n^i$ must be found. We consider a linear expansion of Eq. (1) about the current maxima, $f(x,a) = f(\mu_n,a) + (x-\mu_n)f'(\mu_n,a) + \mathcal{O}[(x-\mu_n)^2]$. The probability in the region $n[f(\mu_n,a)] = [f(\mu_n,a) - \Delta x/2, f(\mu_n,a) + \Delta x/2]$ can be found by assuming uniform density in the region of interest and its pre-image. We find the denominator of Eq. (5) is approximately $[\rho_n(\mu_n)\Delta x]/|f'(\mu_n,a)|$.

Near one of the critical points, a quadratic expansion of Eq. (1) must be used, $f(x,a) = f(x_c^i,a) + 1/2(x-x_c^i)^2 f''(x_c^i,a) + \mathcal{O}[(x-x_c^i)^3]$. As in the above, we consider the probability associated with the neighborhood $n[f(x_c^i,a)]$. If x_c^i is a local maxima, this region is $n[f(x_c^i,a)] = [f(x_c^i,a) - \Delta x, f(x_c^i,a)]$. Again, we assume a uniform density in the region of interest and its pre-image. With these approximations we find the numerator in Eq. (5) is approximately $2\sqrt{(2\Delta x)/|f''(x_c^i,a)|}\rho_n[x_c^i]$. Combining these results, we obtain

$$\mathcal{R}_n^i \approx 2|f'(\mu_n,a)|\sqrt{\frac{2}{\Delta x|f''(\mu_n,a)|}}\frac{\rho_n[x_c^i]}{\rho_n[\mu_n]}. \tag{7}$$

In application of this result, Δx should be set equal to measurement resolution in experiment and bin size in ensemble simulation. We also employ the approximation discussed above, $\rho_n(x) \approx \mathrm{N}(x;\mu_n,\sigma_n)$

One hundred ensemble simulations were performed to test the effectiveness of Eq. (6) and Eq. (7) using the Logistic map. For each simulation a uniform random value on the unit interval was generated, $x_r = \mathrm{rand}[0,1]$. Next, the map was applied for five hundred time steps to ensure a typical value on the attractor and the measured value set, $m_0 = f^{(500)}(x_r,a)$. Finally, a set of $n_d = 2\times 10^6$ initial conditions were generated using a normal distribution, $x_j \sim \mathrm{N}(m_0,\sigma_0)$, where $\sigma_0 = 5\times 10^{-3}$.

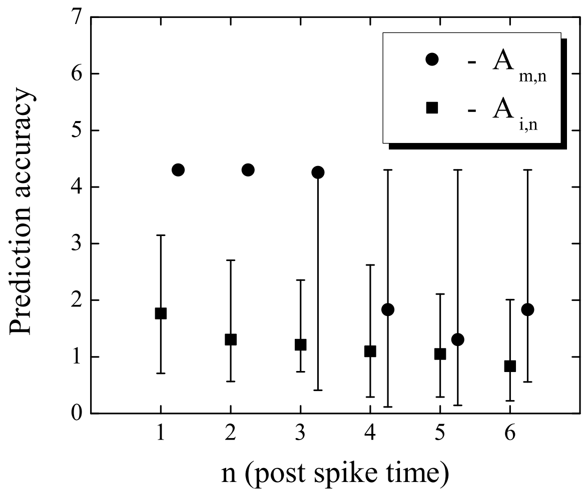

FIG. 2: Prediction accuracy of the proposed algorithm for 100 simulations. Post spike time $n = 1$ corresponds to the first fold in the probability density. Data provided shows the median accuracy with bars which indicate the $(10th, 90th)$-percentiles.

At each time step the most likely trajectory, corresponding to the bin with the largest probability density as given in Eq. (3), is obtained and given the value $h_n = x_i$. For our purposes, the value of h_n is considered to be the true most likely trajectory. Two methods of predicting this value are considered: (1) the image of the initial most likely point, $f^{(n)}(m_0,a)$, and (2) the results of our method, μ_n as given in Eq. (6a).

We define two values which provide a numerical measure of the prediction *accuracy*

$$\mathrm{A_{i,n}} = -\log_{10}|f^{(n)}(m_0,a) - h_n| \tag{8a}$$

$$\mathrm{A_{m,n}} = -\log_{10}|\mu_n - h_n|. \tag{8b}$$

$\mathrm{A_{i,n}}$ describes the accuracy obtained by iterating the measured value with a perfect model and $\mathrm{A_{m,n}}$ the accuracy from application of Eq. (6). In this form, these values reflect the number of decimal places of accuracy for each approach. As a result, larger values reflect a more accurate prediction.

Fig. (2) provides the results of 100 simulations performed for the Logistic map at $a = 3.80$. Only data for post spike time, which starts when the first fold occurs in each simulation, are provided. Before the first fold (not shown), the predictions for $f^{(n)}(m_0,a)$ and μ_n are exactly the same. A value of $\mathrm{A_{i/m,n}} \approx 4$, demonstrates prediction accuracy representative of the histogram resolution,

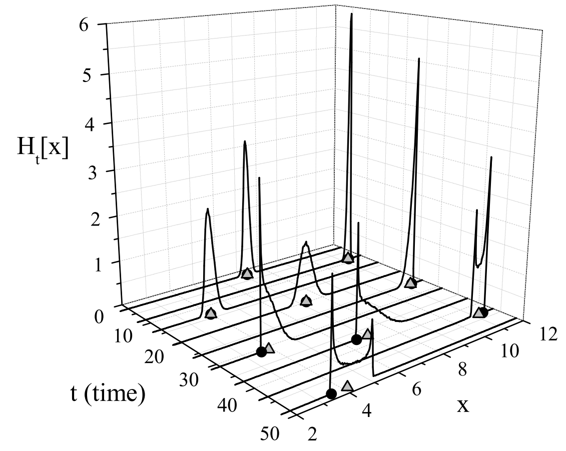

FIG. 3: An example of folding of the probability density in the Rössler attractor. Each time x reaches a local maximum in its dynamics a histogram of the ensemble is shown. The most likely trajectory (black circle) and the path of the initial measurement (gray triangle) are also provided.

$n_b^{-1} = 10^{-4}$. For each prediction method, the median accuracy and bars which show the $(10th, 90th)$-percentiles are provided. The results demonstrate increased prediction accuracy for the proposed method, $\mathrm{A_{m,n}} \geq \mathrm{A_{i,n}}$, for three time steps in 87 of 100 trials conducted.

Next, we discuss two areas of concern regarding the results presented to this point. It is natural to question the application of these ideas in the presence of noise, for example by modifying Eq. (1) to read $x_{n+1} = f(x_n, a) + \epsilon \mathrm{N}(0,1)$. We find this does not affect the results presented here for reasonable noise levels, $\epsilon < 10^{-3}$. Above this level, the noise is sufficient to smooth peaks created by folding and the property we exploit is no longer relevant.

Finally, we address the application of these ideas to a more complicated system. In particular, can the same ideas be used in a system of ordinary differential equations? When we consider the return map generated by the sequence of maxima from one of the variables, often called the *Lorentz* map, we sometimes find a unimodal shape. An example is the Rössler attractor, given by the equations $dx/dt = -y - z$, $dy/dt = x + ay$, and $dz/dt = b + (x - c)z$. If we consider a return map for the sequence of maxima in the x-dynamics, we find the desired properties.

In Fig. (3) we see the evolution of an ensemble of $n_d = 50\,000$ trajectories obtained by 4-th order Runge-Kutta with values $a = 0.2$, $b = 0.2$, $c = 5.7$, and $\mathrm{dt} = 0.01$. As in our analysis of the Logistic map, an ensemble consistent with an initial condition with uncertainty was generated after iterating a random initial state onto the attractor. Each time the x-dynamics reached a maxima, a histogram was created from the ensemble. Folding dynamics are clearly present in the ensemble and we note the most likely trajectory and the evolution of the initial measured value do not agree beyond the short-term. We expect application of the methods we have introduced to extend prediction in this case as well.

In this Letter we have demonstrated that knowledge of ensemble dynamics can be used to extend prediction when there is uncertainty in measurement of the initial condition. A fold can be detected and this information used to adjust the predicted trajectory appropriately. Application to the Logistic map demonstrates the effectiveness of this method and preliminary results using the Rössler attractor demonstrate the potential for application of these ideas to systems of ordinary differential equations.

The authors wish to acknowledge insightful discussions with Joseph Jun and Geoffrey Warner and helpful suggestions in preparing this manuscript from Tim Head and Glenn Foster. This work was supported by National Science Foundation Grants No. NSF PHY 01-40179, NSF DMS 03-25939 ITR, and NSF DGE 03-38215.

[1] N. Gershenfeld, B. Schoner, and E. Metois, Nature **397**, 329 (1999).
[2] V. F. Pisarenko and D. Sornette, Phys. Rev. E **69**, 036122 (2004).
[3] P. E. McSharry and L. A. Smith, Phys. Rev. Lett. **83**, 4285 (1999).
[4] K. Lehnertz and C. E. Elger, Phys. Rev. Lett. **80**, 5019 (1998).
[5] O. N. Bjørnstad and B. T. Grenfell, Science **293**, 638 (2001).
[6] L. M. Hively and V. A. Protopopescu, Chaos **14**, 408 (2004).
[7] J. Harlim et al., Phys. Rev. Lett. **94**, 228501 (2005).
[8] L. A. Smith, Proc. Nat. Acad. Sci. U.S.A. **99**, 2487 (2002).
[9] H. D. I. Abarbanel et al., Rev. Mod. Phys. **65**, 1331 (1993).
[10] J. L. Breeden and A. Hübler, Phys. Rev. A **42**, 5817 (1990).
[11] J. D. Farmer and J. J. Sidorowich, Phys. Rev. Lett. **59**, 845 (1987).
[12] P. Cvitanović, Phys. Rev. Lett. **61**, 2729 (1988).
[13] S. Grossmann and S. Thomae, Z. Naturforsch **32a**, 1353 (1977).
[14] R. F. Fox, Chaos **5**, 619 (1995).
[15] A. Lasota and M. C. Mackey, *Chaos, Fractals, and Noise* (Spring-Verlag, New York, 1994), 2nd ed.
[16] R. May, Nature **261**, 459 (1976).
[17] O. E. Rössler, Phys. Lett. **57A**, 397 (1976).
[18] R. Shaw, Z. Naturforsch **36a**, 80 (1981).